L-PBF and DED processing of a Ni-based superalloy

M Thomas, Eric Charkaluk, Denis Solas, Fabien Szmytka, Didier Locq, Ariel Morel, Olivier Hubert, Nicolas Muller, Christophe Tournier

L-PBF and DED processing of a Ni-based superalloy

M. Thomas[1] marc.thomas@onera.fr; E. Charkaluk[2] eric.charkaluk@polytechnique.edu; D. Solas[3] denis.solas@universite-paris-saclay.fr; F. Szmytka[4] fabien.szmytka@ensta-paris.fr; D. Locq[1] didier.locq@onera.fr; A. Morel[1] ariel.morel@onera.fr; O. Hubert[5] olivier.hubert@ens-paris-saclay.fr; N. Muller[6] nicolas.muller@ens-paris-saclay.fr; C. Tournier[6] christophe.tournier@ens-paris-saclay.fr

[1] (DMAS, ONERA, Université Paris Saclay, F-92322 Châtillon - France)
[2] (Laboratoire de Mécanique des Solides - UMR 7649, Institut Polytechnique de Paris, 91128 Palaiseau, Cedex, France)
[3] (Université Paris-Saclay, CNRS, ICMMO, 91405 Orsay, France)
[4] (ENSTA Paris - Institut Polytechnique de Paris, 91120 Palaiseau, France)
[5] (Université Paris-Saclay, ENS Paris-Saclay, LMPS, 91190, Gif-sur-Yvette, France)
[6] (Université Paris-Saclay, ENS Paris-Saclay, LURPA, 91190, Gif-sur-Yvette, France)

Abstract

Different additive manufacturing (AM) technologies such as L-PBF and DED do become really attractive for both repair and 3D part manufacturing. In particular, extensive work is in progress for the non-weldable nickel-based superalloys which tend to exhibit cracks due to residual stresses build-up during AM thermal cycles. Within the framework of the project FAPS conducted at Université Paris-Saclay, the present investigation will highlight the processing conditions and build-up strategy that produce crack-free specimens for alloy AD730®. The latter was developed by Aubert & Duval for cast&wrought gas turbine applications. In this work, a comparison between such conventional processing and AM will be provided in terms of mechanical performance. The results clearly show an anisotropic behaviour related to the sharp crystallographic texture induced by the epitaxial grain growth. The results will be discussed, with a perspective analysis of maturity for this AM processed-material, the process robustness, the potential technological developments and application prospects.

1. Introduction

In the last years, AM has been observed to be difficult for non-weldable nickel-based superalloys because of their crack sensitivity. Therefore, research efforts have been devoted to a variety of process and alloy composition optimisations, with the postulate that these commercial alloys were not optimised with such severe thermal gradient conditions as experienced by AM. Attempts have been made with significant success on different nickel-based superalloys (Mar-M247, IN738, IN713) by adjusting the process parameters and the build strategy and also by tuning chemical compositions. However, the challenge is that these process and alloy adjustments must not be achieved at the expense of the mechanical performance.

One of the alloys which currently attracts interest, is the so-called AD730® alloy developed by Aubert & Duval for cast&wrought (C&W) applications in the aeronautical sector. This nickel-based superalloy, in its fine grain version, offers a very good properties-versus-cost balance with a high creep and fatigue resistance at elevated temperature. The AD730® alloy was initially developed as a cost-effective version of Udimet720 in terms of alloy chemistry by limiting the presence of expensive elements, in particular lower cobalt content, and by using a significant iron content [1-2]. The processability was also improved by reducing the fraction and the solvus temperature of the γ' phase. The AD730® alloy also offers the advantage of excluding topologically compacted phases (TPC). In the high temperature regime of gas turbine disc (720°C), AD730® alloy exhibits a higher yield stress (YS) than Udimet720.

ONERA, as the French Aerospace Lab, has already been involved in collaborative work with Aubert & Duval for pushing up the temperature limits of conventionally processed AD730® [3]. In the present collaborative work with a number of partners of Université Paris-Saclay, the objective was to develop AD730® alloy by using different AM technologies such as laser power bed fusion (L-PBF) or directed energy deposition (DED). Most of the results presented below concerns the L-PBF process which is considered as the most widespread AM technology for metals studied in the world. By laser melting layer by layer a fine metallic powder, L-PBF offers the advantages of shaping complex parts with good surface roughness by using a great number of metallic alloys [4-5].

The main difficulty is related to the fact that AD730® is considered as a non-weldable nickel-based superalloy consistently with the welding cracking sensitivity diagram that separates the different alloys as a function of their Ti and Al contents, both elements enhancing the formation of strengthened precipitates [6].

Therefore, a primary aim in this study was to determine suitable processing conditions for having sound specimens and for alleviating any cracking tendency. Achieving a good quality for structural parts surely depends on process parameters, but the powder characteristics in terms of powder particle size and morphology also play an important role. Actually, a high powder bed density and a good spreadability is highly recommended, which means the beneficial effect of bimodal particle size distribution and the rejection of extremely fine powder particles. By anticipating successful results with this processing approach to obtain defect-free parts, an industrial motivation was then to mechanically test the alloy compared to cast and wrought (C&W) test specimens and to explore the resulting microstructural characteristics for a better understanding of microstructure - properties relationships.

2. Experimental procedure

Two batches of powders have been supplied by Aubert & Duval: a first batch of powders with a fine particle size (<53 µm) for L-PBF experiments and a second batch of powders with a particle size of 53-106 µm for DED experiments. The particle size distribution (PSD) was determined using a laser particle size analyzer (model Horiba Partica LA_950V2). The compressibility of powders was estimated for both batches by the packing of this powder through the apparent density and the tapped density measurements. The tapped density was determined by measuring the mass and volume of the powder in a graduated cylinder subjected to a vertical tapping using 100 manual shocks. The ratio between the tapped and the apparent densities provides Hausner index values which enable to characterize the powder flowability. Chemical analysis was performed on both batches by using ICP-OES for major elements and by LECO and Inductor ONH for minor elements such as C, B, O, S, N, P.

L-PBF experiments were carried out on a FormUp 350 laser melting machine (AddUp, France) equipped with a 500W ytterbium fiber laser (1065 nm) and a roller coating system. The chamber was protected with argon atmosphere and no preheating system of the plate was used. A precise protocol was established with the build-up of successive single beads, small cubes and finally 3D test specimens.

Mechanical tests were performed on L-PBF specimens in a solution annealed (1080°C for 4 hours followed by argon cooling) + single aged condition (730°C for 8 hours followed by air cooling). The influence of the build orientation was determined by comparing test specimens along the X and Z directions. These results are compared with those obtained for cast&wrought (C&W) AD730® materials: a fine grain microstructure [2] and a coarse grain microstructure [3].

It is recalled that the fine grain microstructure of C&W AD730® is obtained by a sub-solvus annealing at 1080°C for 4 hours followed by oil quenching, and then by an ageing condition at 730°C for 8 hours followed by air cooling. The L-PBF material actually received the same heat treatment, except the argon cooling instead of oil quenching. For the AD730® coarse grain version, the heat treatment corresponds to a super-solvus annealing at 1120°C for 1 hour with a cooling rate of 40°C/min, followed by a sub-solvus annealing at 1080°C for 4 hours with a cooling rate of 100°C/min, and then an additional double-ageing (800°C/4h air cooling + 760°C/8h air cooling).

The heat treatment for the fine grain version yields a mean grain size close to 10 µm and an unimodal γ' precipitate size close to 70 nm [2]. On the other hand, the heat treatment for the coarse grain version results in mean grain size of 140 µm and a bimodal γ' precipitate distribution (mean size of 372 and 106 nm) [3].

Room temperature tensile tests were carried out at a strain rate of 2.5×10^{-4} s^{-1} up to YS and then to a strain rate of 65×10^{-4} s^{-1} up to failure using an MTS-810 displacement controlled tensile machine. A 20-mm extensometer was used to follow the deformation during the tests. Tensile tests were also performed at 650°C, 750°C and 800°C at a uniform strain rate of 10×10^{-4} s^{-1} using a similar MTS-810 displacement controlled tensile machine and a 20-mm extensometer.

Different creep conditions were used to identify a possible difference in creep behaviour in relation to C&W AD730®, as follows: 700°C and 690 MPa, 750°C and 500 MPa, 850°C and 200 MPa.

3. Experimental results

Powder characterisation

Chemical analyses for the two batches of powder are compared to the min and max values of Pearl® Micro AD730. As displayed in Table 1, the alloying element contents are consistent with the chemical range given by Aubert & Duval. Compared to each other, the 10-53 µm and the 53-106 µm powders yield the same alloying element contents, consistently with the fact that both powder batches originate from the same ingot and the same atomisation.

Table 1 – Chemical composition of AD730® alloy (wt%)

Sample	Ni	Cr	Co	Fe	Mo	W	Al	Ti	Nb	C	B	Zr
Pearl® Micro Min values	*Bal.*	*15.00*	*8.00*	*3.00*	*2.50*	*2.30*	*2.00*	*3.20*	*0.80*	*0.003*	*0.005*	*0.001*
Pearl® Micro Max values	*Bal.*	*17.00*	*10.00*	*5.00*	*3.50*	*3.30*	*2.60*	*3.80*	*1.40*	*0.025*	*0.025*	*0.050*
Powder < 53 µm	*Bal.*	*16.16*	*8.26*	*4.12*	*3.16*	*2.61*	*2.46*	*3.56*	*1.05*	-	*0.010*	*0.020*
Powder 53-106 µm	*Bal.*	*16.25*	*8.36*	*4.16*	*3.21*	*2.68*	*2.51*	*3.56*	*1.04*	-	*0.010*	*0.050*

In the case of powder <53 µm which is of main interest for L-PBF, the PSD is well centered between the extreme values, namely 10 and 53 µm, with only 2.45% of powder off range (>53 µm).

The apparent density and the tapped density were measured by using 50 g of powders. The Hausner index corresponds to the ratio of the tapped density over the apparent density. This can also be expressed by the ratio of the apparent volume over the tapped volume. The apparent volume, the tapped volume and the Hausner index are gathered in Table 2 for the two batches of powder. These measurements do confirm that both batches exhibit a good powder flowability.

Table 2 – Density measurements of AD730 powders

Powder	$V_{apparent}$ (cm^3)	V_{tapped} (cm^3)	Hausner index
< 53 µm*(1)*	10.37	9.12	1.14
53-106 µm*(2)*	22.53	19.43	1.16

(1) Sample 25 ml – (2) Sample 100 ml

L-PBF experiments

Designs of experiments were carried out to determine the best process parameters for L-PBF, starting with the manufacturing recipes for a well-known nickel-based superalloy, i.e. the IN718. The standard condition for this alloy was a power P_0 = 210 W and a scanning speed V_0 = 1800 $m.s^{-1}$.

Three sets of 10 mm × 10 mm section blocks were successively produced with a ± 10% variation from the initial parameters P_0 and V_0 (figure 1-a) and then from the best produced block. The quality criteria are based on the geometrical and metallurgical characteristics of the samples. In particular, the absence of cracks and a porosity rate as low as 0.1% in a 1 mm^2 area that includes multilayers and interlayers were controlled to refine the values of the process parameters. Other parameters such as the layer thickness t and the hatching distance h were also taken into consideration for the selection of the best conditions.

In the present work, a single build strategy was selected for microstructural and mechanical characterisation. Considering the build direction as the Z-axis, the laser scanning strategy consisted in a contour with unidirectional filling at 45° or - 45° from the X-axis from layer-to-layer. The scan vector rotation allows reducing residual stress formation and improve mechanical properties compared to

constant vector direction over the layers [7]. Various specimens were produced in the X, Y and Z directions with geometries adapted to the characterisations performed (figure 1-b). Specimens were then machined and post-heat treated.

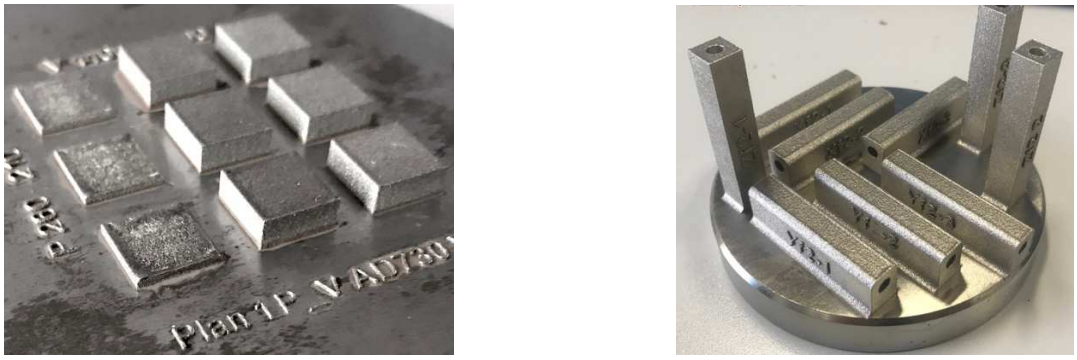

(a) (b)

Figure 1: (a) blocks produced during the first iteration including three blocks for which the process parameters could not ensure the production (specific energy P/V too high) ; (b) Testing specimens produced along the X, Y and Z directions on the base plate

Microstructure and texture analysis

Several 10 mm × 10 mm × 10 mm blocks were cut along the YZ and XY planes for microstructure and texture investigations. Areas of 1 mm x 1 mm with 0.5 µm step size were quantitatively analysed by using Electron Backscatter Diffraction (EBSD) in a Scanning Electron Microscope. As induced by the scanning strategy, crystal orientation maps in XY and YZ planes which are illustrated in Figure 2-a, exhibit a strong morphological and crystallographical texture. Whereas a classical chessboard morphology is observed along XY plane, a columnar structure tends to develop along the Z-axis in the YZ plane, showing the influence of thermal gradients along Z direction and thus enhancing the epitaxial grain growth with successive layers. The major red colors of grains in both XY and YZ are indicative of a strong crystallographic [001] orientation which is close to a single-crystalline-like cube texture rotated along the Z direction by 45°, as induced by the scanning vectors strategy with a 90° rotation between the layers (Figure 2-b). The microstructure also shows a limited number of high angle grain boundaries (HAGB).

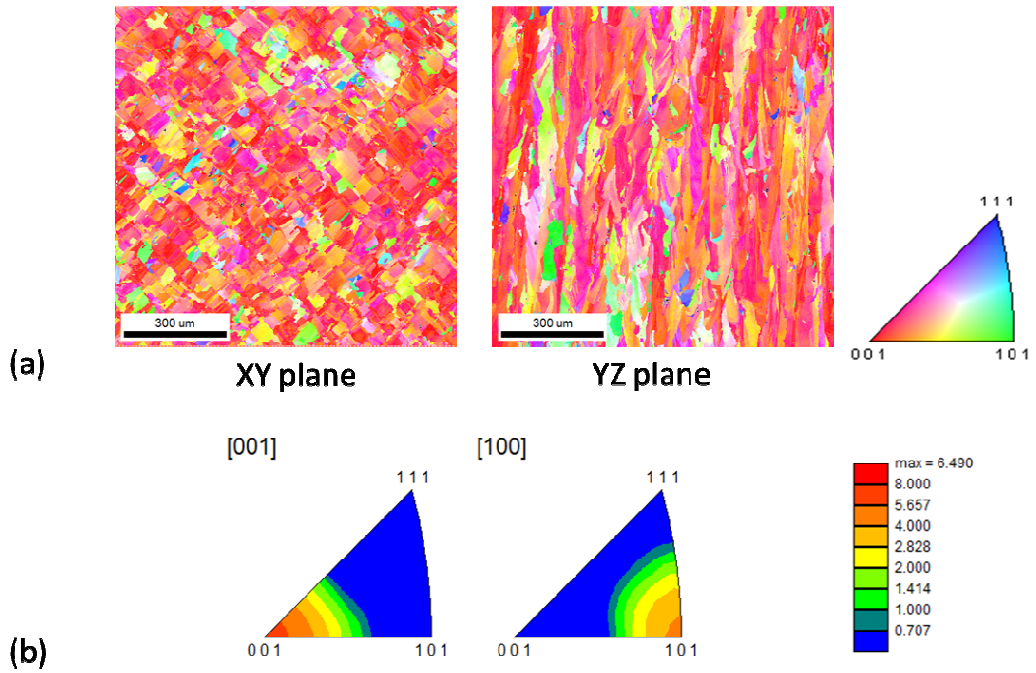

Figure 2: (a) Crystal orientation maps in XY and YZ plane (The color shows the crystal direction parallel to the building direction) and (b) Z and X inverse pole figures.

Attempts to quantify the anisotropy of mechanical properties were made by means of a self-consistent approach based on the determination of a discrete distribution of orientations with weight (grain size), as deduced from EBSD analyses. As a first approximation, the single crystal elastic constants were estimated to be: C11 = 247 GPa, C12 = 153 GPa and C44 = 122 GPa (pure nickel). Then, the elastic stiffness was calculated and Young's modulus anisotropy was deduced. The orientation dependence of the stiffness is clearly visible in Figure 3 where a comparison with a single crystal or a random (isotropic) texture is provided, showing E values for the sample of 150 GPa and 200 GPa along the Z and Y orientations, respectively.

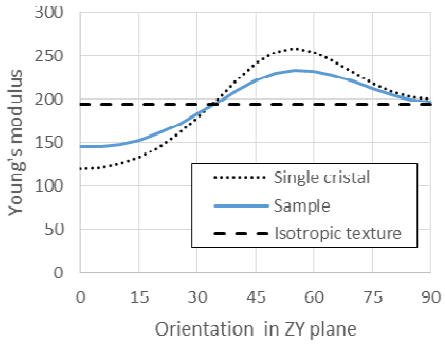

Figure 3 : Anisotropy of the Young's modulus in the YZ plane.

The grain orientations of the test specimen appear to be relatively closed to a single-crystalline texture with less than 15° spreading. Therefore, one may consider that the Young's modulus anisotropy of the specimen shows a similar evolution than a single crystal but with a lower amplitude. It can be deduced that the lowest value in tension along the Z axis corresponds to the [0 0 1] orientation of columnar grains, whereas the highest value at 55° corresponds to a [1 1 1] orientation.

Microstructural investigations were also made at high magnification to compare with C&W conditions. Here, the first condition is referred to a C&W material having fine grains, typically 10-15 µm in size. Moreover, this alloy exhibits a high density of very fine γ' precipitates which are beneficial for mechanical strength. The second condition corresponds to a C&W material with a coarse grain microstructure, typically 140 µm in size, and with a bimodal distribution of γ' precipitates, more specifically for the creep resistance. In contrast, the L-PBF AD730® microstructure is characterised by very fine grains of approximately 5 µm and by coarser grains up to 100 µm as illustrated in Figure 4.

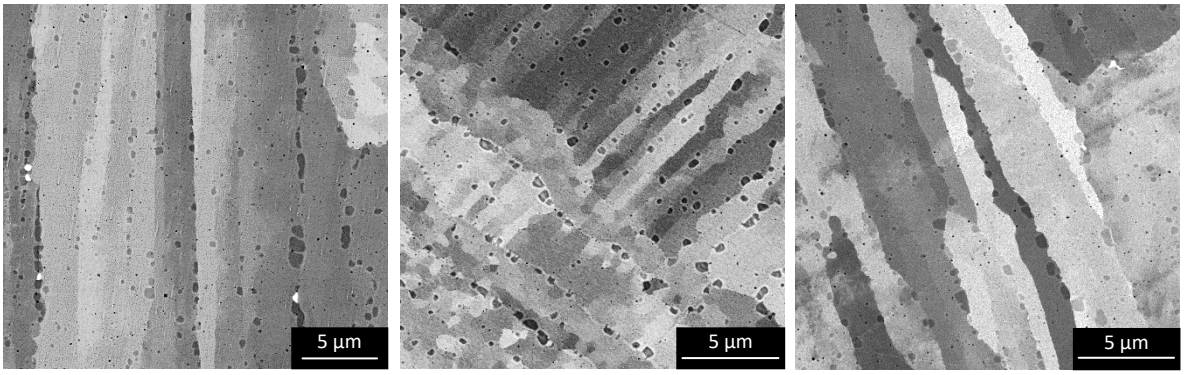

(a) (b) (c)

Figure 4 : SEM micrographs in back-scattered electron mode, showing the fine microstructure. L-PBF AD730® alloy: (a) XZ plane, (b) XY plane, (c) YZ plane

Subsequent argon cooling leads to the precipitation of small secondary γ' which are mainly transgranular. A coalescence of these secondary γ' precipitates occurs during subsequent ageing at 730°C for 8 hours as observed in Figure 5.

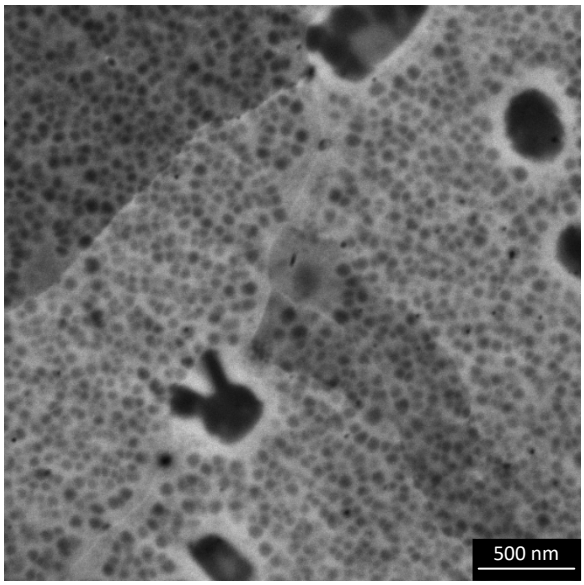

Figure 5 : SEM micrograph in back-scattered electron mode, showing fine secondary γ' precipitates and depleted zones around coarser primary γ' precipitates in the XY plane

Tensile properties

Room-temperature tensile properties of L-PBF AD730® alloy are displayed in Table 3 with three duplicated tests for each orientation. As expected from the tensile elongation values, no evidence of premature failure has been noticed which might be relevant of the presence of micro-cracks. It must be pointed out that this behaviour is in contrast with previous work showing a severe cracking sensitivity for this alloy through AM processing [8]. This encouraging result in the present work is attributed to the set of process parameters that were chosen to develop a particularly fine and textured microstructure.

Table 3 – Room temperature tensile properties of L-PBF AD730® alloy for both orientations

Orientation	**X**	**Z**
Young's modulus (GPa)	230	150
Yield stress (MPa)	1160	1100
Ultimate tensile strength (MPa)	1450	1410
Total elongation (pct)	21 pct	14 pct

As expected from the EBSD texture analysis, the L-PBF material exhibits a strong anisotropic tensile behaviour with significantly higher properties in the X orientation (Table 3). The AD730® alloy is considerably stiffer in the X orientation compared to the build direction. An important work hardening of approximately 300 MPa is observed for both orientations, which is presumably attributed to strong interactions between existing microstructural features and an increasing dislocation density occurring from plastic deformation.

The evolution of tensile properties with test temperature is illustrated in Figure 6 by normalizing with respect to C&W fine grain version. The large difference in Young's modulus for X and Z orientations remains approximately the same at 700 and 750°C (Fig. 6a). The X orientation yields slightly higher values than those of the C&W coarse and fine grain versions. Now, regarding YS at high temperature, both orientations of the L-PBF material lie between the coarse and fine microstructures of C&W

AD730®. Based on the fact that the C&W fine grain version received approximately the same heat treatment as the L-PBF AD730®, which means the same occurrence of γ' precipitation, then the difference in YS might be related to a grain size dependence. On the other hand, the lower YS for the C&W coarse grain version should be mainly attributed to coarser γ' precipitates.

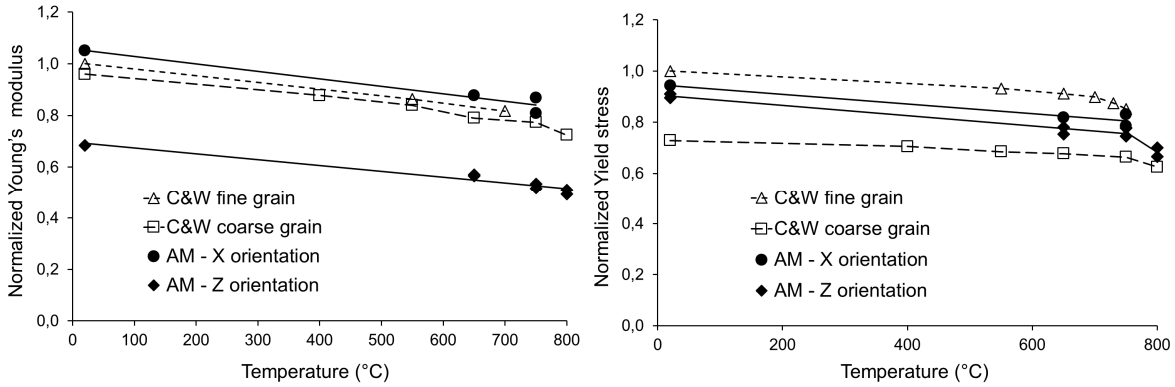

Figure 6 : Effect of the build orientation and the microstructure on high temperature tensile properties; (a) Normalized Young's modulus with respect to C&W fine grain version; (b) Normalized Yield stress with respect to C&W fine grain version

The creep behaviour of AD730® processed by L-PBF was investigated by conducting deformation creep tests from 700°C to 850°C in comparison with conventionally processed AD730®. The Larson-Miller representation clearly shows a stress dependence to determine which microstructure has the best creep properties (Fig. 7). As expected, the C&W coarse grain version is much more creep resistant than the C&W fine grain version. However, the difference in creep is dramatically reduced as the applied stress is increased and the temperature is concomitantly decreased. In the low stress regime, the C&W AD730® is strongly microstructure dependent with the occurrence at high temperature of grain boundary sliding for the fine grain version. In the high stress regime and lower temperature, creep tends to be governed by the strength of the alloy which is in favour of the C&W fine grain version.

Now, regarding the L-PBF material, specimens cut along the Z orientation show a very good creep resistance, quite similar to that of C&W coarse grain. On the other hand, the creep resistance is significantly lower for specimens cut along the X orientation, but still remaining above that of C&W fine grain. This is consistent with the fact that the YS at elevated temperature is higher for X orientation than for Z orientation, which results in a YS / applied stress ratio more favourable for X orientation, thus leading to values which are close to each other for high applied stress such as 690 MPa.

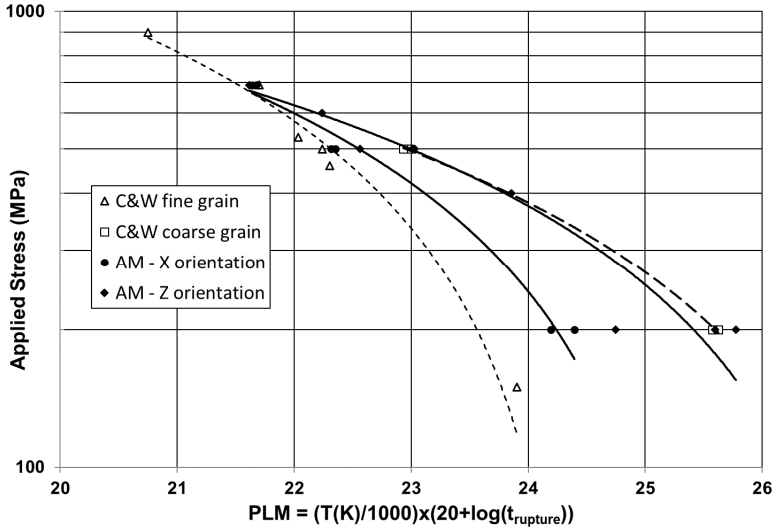

Figure 7 : Larson-Miller representation showing the creep resistance of C&W and L-PBF AD730®

4. Conclusion

An extended characterisation is currently made for the AD730® alloy processed by L-PBF and DED in order to evaluate the potentialities of the AM route compared to C&W for gas turbine applications. In the present paper, the experimental results have been focused on microstructure and mechanical properties of L-PBF AD730®. A major trend of this study is that a specific set of process parameters enables to produce crack-free samples with a low porosity rate. This is achieved by using a specific laser scanning strategy which enhances the epitaxial growth along the build direction as to design a highly textured microstructure with only a few high angle grain boundaries (HAGB). The L-PBF process robustness is highly encouraging since there was not the slightest premature failure among several dozen of test specimens. Post-heat treatments were successfully applied to trigger a homogeneous primary and secondary γ' precipitation. Despite the considerably higher stiffness in the X orientation compared to the build direction, the latter is the preferred orientation in terms of high temperature properties, in particular for gas turbine disc applications. The L-PBF AD730® alloy exhibits a similar creep resistance along the Z orientation as the one of the C&W coarse grain version. Complementary tests are in progress to evaluate the fatigue life and the environmental resistance of the L-PBF AD730® alloy with respect to the C&W counterparts and to compare L-PBF versus DED for AD730®.

Acknowledgements

We would like to thank Pierre-François Giroux from CEA for his valuable contribution to perform every heat treatments in this work. Special thanks are also expressed to the Département génie mécanique at ENS Paris-Saclay for machining test specimens. Technical support of Catherine Rio from ONERA is also gratefully acknowledged for SEM investigations. The authors also express their gratitude to the company AddUp for providing helpful suggestions for the development of design of experiments.

References

[1] A. Devaux, E. Georges, P. Héritier., Advanced Materials Research, Vol. 278 (2011) pp 405-410.

[2] A. Devaux, A. Helstroffer, J. Cormier, P. Villechaise, J. Douin, M. Hantcherli, F. Pettinari-Sturmel, Effect of aging heat-treatment on mechanical properties of AD730^{TM} superalloy, in 8th International Symposium on Superlloy 718 and Derivatives, TMS, 2014.

[3] D. Locq, C. Ramusat, J.-M. Franchet, A. Devaux, Coarse grain C&W AD730 disk superalloy for high temperature applications, work presented at Journées Annuelles SF2M 2016, Paris, France, 2019 (https://hal.archives-ouvertes.fr/hal-02486871).

[4] DD. Gu, W. Meiners, K. Wissenbach, R. Poprawe, Laser additive manufacturing of metallic components: materials, processes and mechanisms. Int Mater Rev 2012;57:133–64. https://doi.org/10.1179/1743280411Y.0000000014.

[5] WE. Frazier, Metal additive manufacturing: a review. J Mater Eng Perform 2014;23:1917–28. https://doi.org/10.1007/s11665-014-0958-z.

[6] Y. Danis, Etude de la soudabilité d'un superalliage base nickel fortement chargé en éléments durcissants titane et aluminium : l'inconel 738. Université de Bordeaux, 2008.

[7] H. Ali, H. Ghadbeigi, and K. Mumtaz. Effect of scanning strategies on residual stress and mechanical properties of selective laser melted Ti6Al4V. Materials Science and Engineering: A, 712:175–187, 2018.

[8] A. Després, S. Antonov, C. Mayer, C. Tassin, M. Veron, J-J. Blandin, P. Kontis, G. Martin, On the role of boron, carbon and zirconium on hot cracking and creep resistance of an additively manufactured polycrystalline superalloy, Materialia, Volume 19, 2021, 101193.